separations

MDPI

Article

Multidimensional Quality Evaluation of Drying Methods on the Bioactive Components and Antioxidant Activity of *Astragalus membranaceus* var. *mongholicus* Slices

Feifan Leng [1], Jiale Wang [1,2], Lizhe Hu [2,3], Minmin Li [4], Yongwei Sun [3], Yonggang Wang [1], Jieyin Chen [2,5], Xiaofeng Dai [2], Bin Ma [6,*], Qing Lv [7,*] and Zhiqiang Kong [2,*]

1 School of Life Science and Engineering, Lanzhou University of Technology, Lanzhou 730050, China
2 State Key Laboratory for Biology of Plant Diseases and Insect Pests, Institute of Plant Protection, Chinese Academy of Agricultural Sciences, Beijing 100193, China
3 College of Life Sciences, Inner Mongolia University, Hohhot 010021, China
4 Key Laboratory of Agro-Products Quality and Safety Control in Storage and Transport Process, Ministry of Agriculture and Rural Affairs/Institute of Food Science and Technology, Chinese Academy of Agricultural Sciences, Beijing 100193, China
5 Western Agricultural Research Center, Chinese Academy of Agricultural Sciences, Changji 831100, China
6 Institute of Forestry and Grassland Ecology, Ningxia Academy of Agricultural and Forestry Sciences, Yinchuan 750002, China
7 Institute of Industrial and Consumer Product Safety, Chinese Academy of Quality and Inspection & Testing, Beijing 100176, China
* Correspondence: mbin89@163.com (B.M.); lvqing2009@126.com (Q.L.); kongzhiqiang@caas.cn (Z.K.)

Abstract

This study systematically evaluated the effects of five drying methods (sun drying, freeze drying, shade drying, and hot air drying at 40 °C and 60 °C) on the multidimensional quality of *Astragalus membranaceus* var. *mongholicus* slices using multiscale techniques and multivariate analysis. The results showed that the drying methods significantly influenced color, microstructure, volatile organic compound profiles, the content of 13 bioactive constituents, and antioxidant activity. Among all treatments, hot air drying at 40 °C achieved the highest composite score in the comprehensive evaluation. This treatment was associated with a marked increase in surface microroughness (Ra), higher levels of the pharmacopoeial markers astragaloside IV and calycosin-7-O-β-D-glucoside, and enhanced ABTS radical scavenging activity. However, other methods performed better in individual parameters: shade drying showed higher DPPH and FRAP values, while freeze drying gave the highest total phenolic content. Based on the observed strong correlations (e.g., roughness vs. astragaloside IV: r = 0.94; astragaloside IV vs. ABTS: r = 0.83), we propose a testable hypothesis that hot air drying at 40 °C may influence bioactivity partly through physical microstructural changes. The multidimensional evaluation framework established here provides a methodological reference for quality optimization of medicinal and edible herbs.

Keywords: *Astragalus membranaceus* var. *mongholicus*; drying process; quality; multiscale techniques; multivariate analysis

Academic Editor: Gavino Sanna

Received: 7 April 2026
Revised: 5 May 2026
Accepted: 8 May 2026
Published: 11 May 2026

1. Introduction

Astragalus membranaceus (Fisch.) Bge. var. *mongholicus* (Bge.) Hsiao is a medicinal plant from the genus *Astragalus* (family Fabaceae). For thousands of years, the roots of *Astragalus membranaceus* have been widely used in traditional Chinese medicine [1].

The active constituents in *Astragalus membranaceus* are extremely abundant, with over 100 types of bioactive compounds having been isolated and identified so far [2]. Common active constituents include saponins, flavonoids, phenols, and other constituents. These constituents give *Astragalus membranaceus* its diverse pharmacological effects, including anti-obesity, anti-cancer, anti-diabetic, anti-inflammatory, and antioxidant properties [3,4]. In November 2023, China officially included *Astragalus membranaceus* in the list of medicinal and edible substances [5], and in recent years, the application of *Astragalus membranaceus* in the food industry has gradually expanded, being processed into various health beverages, herbal teas, and functional yogurts [6].

To ensure the safety and functionality of these applications, proper manufacturing processes are essential. Drying is a critical step because it removes moisture, extends shelf life, and significantly affects pharmacological activity [7,8]. Commonly used drying methods include sun drying, hot air drying, freeze drying and shade drying. Numerous studies on other medicinal herbs have shown that the choice of drying method has a significant impact on product quality. For example, repeated steaming and drying can enhance the anti-inflammatory activity of *Rehmannia glutinosa* polysaccharides [9]; hot-air-dried extracts of *Bletilla striata* exhibit stronger reducing capacity than naturally dried samples [10]; for *ginseng*, samples dried using far-infrared or vacuum drying had higher total phenolic and flavonoid content than those dried using freeze drying or hot air drying [11]. However, these studies are all species-specific and typically focus on only one or two quality indicators. Drying conditions and evaluation parameters vary widely, making direct comparisons difficult. Most importantly, there has been no systematic research to date examining how different drying methods affect the overall quality of *Astragalus membranaceus* in terms of its chemical, physical, and bioactive properties.

The quality assessment of dried herbal medicines is, by its very nature, multidimensional and comprehensive. It requires researchers to simultaneously focus on the chemical components directly related to efficacy, the physical properties that affect processing and storage stability (such as color and microstructure), and biological activity, which serves as a core functional indicator [12,13]. Traditional evaluation methods often rely solely on a single metric or a limited set of parameters and thus fail to fully reflect a product's overall quality characteristics. For example, Li et al. found that, while all three drying methods increased the total saponin and polysaccharide content of *Panax notoginseng*, they reduced its functional activity to varying degrees [14]. To address this shortcoming, we propose a multiscale evaluation framework comprising five complementary evaluation dimensions: color, a marker of the Maillard reaction and enzymatic browning [15]; microstructure, a key factor determining rehydration rate and extraction efficiency [16]; volatile compounds, which contribute to aroma and potential bioactivity [17]; major bioactive compounds, the direct material basis for pharmacological effects [17]; antioxidant activity, a representative indicator for measuring biological effects [18]. By comprehensively measuring all five dimensions, we can determine whether these indicators exhibit synergistic or divergent changes across different drying methods. Furthermore, we will use multivariate analysis methods (PCA, OPLS-DA, heatmaps, and radar charts) to integrate these variables, thereby overcoming the limitations of comparisons based on a single metric.

Specifically, this study aims to investigate how five drying methods (SD, HAD40, HAD60, FD, and SHD) affect the color, microstructure, volatile compounds, bioactive components, and antioxidant activity of *Astragalus membranaceus* var. *mongholicus* root slices. Are there significant correlations among these five dimensions? Under the comprehensive evaluation framework, which drying method ranks first? To address these questions, we characterized the samples across five dimensions using Digieye imaging technology, field

emission scanning electron microscopy (FE-SEM), 3D topography analysis, GC×GC-IMS, and UPLC-MS/MS and performed multivariate analysis.

2. Materials and Methods

2.1. Chemicals and Reagents

The standards for the 13 activate constituents (including calycosin-7-O-β-D-glucoside, liquiritigenin, ononin, apigenin-7-O-β-D-glucoside, orientin, brachyoside B, isoastragaloside I, isoastragaloside II, astragaloside I, astragaloside II, astragaloside IV, soyasaponin I and soyasaponin II) were solid reagents with purity greater than 94% purchased from Tianjin Alta Technology (Tianjin, China) and were configured to 100 μg/mL for use. Mass spectrometry methanol was obtained from Thermo Fisher Scientific (Waltham, MA, USA); analytically pure anhydrous ethanol was purchased from Beijing Tongguang Fine Chemical Co., Ltd. (Beijing, China); 2-butanone, 2-pentanone, 2-hexanone, 2-heptanone, 2-octanone, and 2-nonanone were all of analytical grade for GC-IMS analysis and provided by Aladdin Company (Shanghai, China); ultrapure water is produced by the Milli-Q ultrapure water system manufactured by Merck Millipore (Darmstadt, Germany).

2.2. Sample Source and Drying Procedure

The fresh root of *Astragalus membranaceus* var. *mongholicus* was collected from Yanchi County, Wuzhong City, Ningxia Hui Autonomous Region, China. It was identified as *Astragalus membranaceus* (Fisch.) Bge. var. *mongholicus* (Bge.) Hsiao by Professor Kong of the Institute of Plant Protection, Chinese Academy of Agricultural Sciences, in accordance with the 2025 edition of the Chinese Pharmacopoeia [5]. After washing, the sectioning guide was adjusted to 3 mm, and a microtome was used to slice the samples. The slices were mixed thoroughly and set aside. The thickness of the slices was measured with a vernier caliper and found to be 2–5 mm. These slices were dried using different drying methods (SD, FD, SHD, HAD40, and HAD60). The experiment was conducted with three biological replicates, each of which included three independent technical replicates. All drying procedures are terminated when the sample has dried to constant weight and its moisture content is found to comply with pharmacopoeial requirements, thereby determining the drying time. The drying methods are as follows: for SD, 200 g of fresh slices were placed on a tray in direct sunlight and dried for 3 days at 21–35 °C, 52% relative humidity, and under light breeze conditions (2–3 on the Beaufort scale); for SHD, 200 g of fresh slices were placed on a tray and dried for 4 days in a cool (20–24 °C, 52% relative humidity), well-ventilated, and light-protected indoor environment; for FD, 200 g of fresh slices were placed in a culture dish, covered with plastic wrap (with a few small holes punctured in it), and then dried in a freeze dryer at −50 °C under a vacuum of <10 Pa for 12 h; for HAD40 and HAD60, 200 g of fresh slices were placed on a tray and dried in a blast dryer (Yiheng Scientific Instruments Co., Ltd., Shanghai, China) at 40 °C (for 12 h) and 60 °C (for 10 h), respectively, with forced air circulation.

The 2025 edition of the Chinese Pharmacopoeia stipulates that the moisture content in *Astragalus membranaceus* decoction pieces shall not exceed 10%. Therefore, the moisture content of the dried herbal slices was determined using Method II (Drying Method) under General Rule 0832 of the Chinese Pharmacopoeia [5]. The results showed that the moisture content of FS was 63.4%, and all five drying methods met the pharmacopoeia standards (SD: 6.9%, FD: 4.5%, SHD: 8.8%, HAD40: 5.7%, HAD60: 3.3%). Because there are significant differences in moisture content among different dried samples, all subsequent experiments are based on the dry weight of the dried samples (fresh samples are used for reference only). Dry weight = wet weight × (1 − moisture content).

2.3. Color Determination

The color characteristics of *Astragalus membranaceus* var. *mongholicus* slices were detected using the Digieye Digital Imaging System (Verivide, Leicester, UK). Before each test, automatic calibration should be performed using a standard whiteboard. The total color difference (ΔE) = $[(L_0^* - L^*)^2 + (a_0^* - a^*)^2 + (b_0^* - b^*)^2]^{1/2}$, where L_0^*, a_0^* and b_0^* refer to the lightness, redness and yellowness of the corresponding *Astragalus membranaceus* var. *mongholicus* slices [19].

2.4. Microstructural Analysis of Astragalus membranaceus var. mongholicus Slices

2.4.1. Field Emission Scanning Electron Microscopy (FE-SEM) Analysis

The microstructure of *Astragalus membranaceus* var. *mongholicus* slices subjected to different drying methods was examined using a Gemini300 FE-SEM (Carl Zeiss, Oberkochen, Germany). Only slices of 3 mm thickness and uniform size were selected. To obtain better scanning electron microscope images, the sliced samples need to be sputter-coated with gold to enhance their electrical and thermal conductivity. The cross-section of the slice was examined. Three biological replicates per drying method were used. From each biological replicate, one slice with a uniform thickness of 3 mm was selected. Two representative areas on the cross-section of that slice were randomly selected, and each area was imaged at four magnifications (100×, 200×, 500×, 1000×), yielding 8 images per slice. For statistical comparison of microstructure observations, qualitative assessments (e.g., vascular density, starch granule visibility) were consistently observed across all three biological replicates; no quantitative image analysis was performed for these descriptive observations. FE-SEM parameters: acceleration voltage = 5.00 kV, working distance = 6–8 mm (adjusted for surface flatness), SE2 detector (Signal A). The specific experimental steps refer to the method of [19].

2.4.2. 3D Topography Measurement

The 3D surface structure of *Astragalus membranaceus* var. *mongholicus* slices was analyzed using a GT-X 3D topography profiler (Bruker, Billerica, MA, USA) subjected to different drying methods, and the average surface roughness (Ra) of the slices was recorded. Only slices with a uniform thickness of 3 mm and consistent size were selected. The scanning area was the cut surface of each slice, with a fixed field of view of 1.9 mm × 2.5 mm. All topographic images were acquired at the same lateral resolution (5 μm/pixel) and vertical resolution (0.1 μm), under identical visualization settings (unified Z-axis scaling and color mapping). For each drying method, three biological replicates were performed. The Ra value was obtained from a single scan per replicate, and the final Ra for each group was calculated as the mean ± standard deviation of these three measurements. The specific experimental steps refer to the method of [19].

2.5. Measurement of Antioxidant Capacity

The antioxidant capacity of *Astragalus membranaceus* var. *mongholicus* slices was evaluated by measuring 2,2-diphenyl-1-picrylhydrazyl (DPPH) radical scavenging activity, 2,2′-azino-bis(3-ethylbenzothiazoline-6-sulfonic acid) (ABTS) radical scavenging activity, and ferric reducing antioxidant power (FRAP). For the DPPH and ABTS assays, the antioxidant activity was expressed as the percentage of radical scavenging inhibition. For the FRAP assay, the total antioxidant capacity was calculated as μmol Trolox equivalents per gram dry weight (μmol trolox/g DW). All assays were performed using commercial kits (Suzhou Comin Biotechnology Co., Ltd., Suzhou, China) following the manufacturer's protocols. The detailed procedures are provided in Supplementary Materials S1.1–S1.3. Total phenols, total sugars and total flavonoids were determined using kits from Beijing Solarbio Science & Technology Co., Ltd., Beijing, China (Supplementary Materials S1.4–S1.6).

2.6. Detection of Active Constituents

The detection of the 13 target active constituents in each sample strictly followed the established analytical procedures. Separation and detection were achieved using a liquid chromatography–tandem mass spectrometry (LC-MS/MS) system configured with an CORTECS® UPLC® C18 column (2.1 mm × 100 mm, 1.6 μm, Waters, Milford, MA, USA) and a triple-quadrupole mass spectrometer (Xevo TQ-S micro, Waters, Milford, MA, USA). Detection was carried out in positive electrospray ionization (ESI+) mode with multiple reaction monitoring (MRM), applying a capillary voltage of 3.5 kV. To ensure the transparency of the method and reproducibility of the results, the specific operating procedures for this UPLC-MS/MS method are fully documented in Supplementary Materials S2. The calibration parameters, regression equations, and sensitivities for the 13 active ingredients are listed in Supplementary Materials Table S1.

2.7. Detection of Volatile Substances

Accurately, 1.0 g of dry-weight homogenized powder of *Astragalus membranaceus* var. *mongholicus* was weighed and placed into a 20 mL headspace vial. The vial was sealed and incubated at 80 °C for 15 min, after which analysis by gas chromatography–ion mobility spectrometry (GC-IMS) was performed. The automated headspace sampler was operated under the following conditions: an incubation temperature of 80 °C; an incubation time of 15 min; an injection volume of 500 μL; splitless injection mode; an incubation speed of 500 r/min; and a syringe temperature of 85 °C. The analytes were introduced into a gas phase ion mobility spectrometer (FlavourSpec® from G.A.S., Dortmund, Germany) for separation. The volatile compounds were analyzed by GC-IMS equipped with a capillary column (MXT-WAX, 30 m × 0.53 mm, 1.0 μm, Restek Corporation, Bellefonte, PA, USA). The column temperature was maintained at 60 °C, and high-purity nitrogen (purity ≥ 99.999%) was used as the carrier gas. The flow rate was programmed as follows: an initial flow rate of 2.0 mL/min was held for 2 min, then linearly increased to 10.0 mL/min over 8 min, further increased to 100.0 mL/min over 10 min, and finally held for 10 min. The total run time was 30 min. The inlet temperature was set to 80 °C. The IMS instrument was set with the following parameters: a tritium source was used as the ionization source; the drift tube length was 98 mm; the electric field strength was 500 V/cm; the drift tube temperature was maintained at 45 °C; high-purity nitrogen (purity ≥ 99.999%) was used as the drift gas at a flow rate of 150.0 mL/min; and detection was carried out in positive ion mode. Three biological replicates were used.

Explanation of compound identification confidence: a mixed standard solution containing six ketones (2-butanone, 2-pentanone, 2-hexanone, 2-heptanone, 2-octanone, and 2-nonanone) was used. Calibration curves for retention time and retention index were established. The retention index of the target compound was then calculated based on its retention time. Qualitative analysis of the target compound was performed by searching and comparing results against the GC retention index (NIST 2020) database and the IMS migration time database built into the VOCal software (Version 0.4.10). The acceptance criteria for a positive identification were set as follows: retention index (RI) deviation ≤ ±10, drift time (Dt) deviation ≤ ±1%, and VOCal software match score ≥ 700 (on a scale of 0–1000). According to the recommendations of the Metabolomics Standards Initiative, this level of identification corresponds to Level 2 (putative identification) [20]. This study did not use chemical standards to confirm the compounds at Level 1. Structural confirmation of key differentiating compounds will be further validated using standards in subsequent studies.

2.8. Data Analysis

Histograms were generated using Origin 2021 (OriginLab, Northampton, MA, USA). Statistical significance was defined as $p < 0.05$. Principal component analysis (PCA) of attribute components and evaluation metrics of *Astragalus membranaceus* var. *mongholicus* slices, heatmaps, and analysis of functional modules of interoperability networks were performed using R 4.3.3 software and the following software packages: tidyverse (data processing and visualization), corrplot (heatmap generation), grid and ggplot2 (graphics), paran and boot (parallel analysis and bootstrapping of PCA), factoextra (PCA visualization), and ggrepel (label localization). GC-IMS was performed using the built-in GC of the VOCal software. A retention index (NIST 2020) database and the IMS migration time database were used for searching and comparing to characterize the target substances. Reporter, Gallery Plot, and Dynamic PCA plug-ins in VOCal data processing software were utilized to generate 3D spectra, 2D spectra, difference spectra, fingerprints, and PCA plots of volatile constituents, respectively, for the comparison of VOCs among samples. Orthogonal partial least squares discriminant analysis (OPLS-DA) was performed using SIMCA 14.1 software to assess the relationships between the different drying treatment groups. Raw peak intensity data were TIC-normalized, log10-transformed, and UV-scaled prior to OPLS-DA. Model parameters were set to default values unless otherwise stated. Radargrams for the integrated assessment were generated using the online tool OmicStudio (https://www.omicstudio.cn/tool (accessed on 17 June 2025)).

3. Results and Discussion

3.1. The Influence of Different Drying Methods on the Color Characteristics of Astragalus membranaceus var. mongholicus Slices

Color has always been a visual indicator for herbalists and pharmacists to quickly assess the quality of herbs. The appearance of *Astragalus membranaceus* var. *mongholicus* slices after different drying treatments is shown in Figure S1. The color characteristics of *Astragalus membranaceus* var. *mongholicus* slices under different drying treatments are shown in Table 1. After HAD60 treatment, L* of the slices decreased significantly, followed by HAD40, while the FD-treated slices exhibited a relatively brighter color. As the temperature rises, the Maillard reaction between reducing sugars and amino acids proceeds more rapidly, generating brown pigments (melanoidins) and thereby lowering L value [21]. Therefore, compared to FD processing, the higher drying temperatures of the HAD60 and HAD40 are likely the reason for the lower brightness of the slices [15,22].

Table 1. Color characteristics of different drying methods of *Astragalus membranaceus* var. *mongholicus* slices.

Samples	Color Parameters			Total Color Change
	L*	a*	b*	ΔE
FS	80.99 ± 2.68^{bc}	9.55 ± 1.00^{a}	26.97 ± 2.14^{c}	-
FD	90.04 ± 2.52^{a}	5.08 ± 1.53^{c}	19.78 ± 3.16^{d}	12.73 ± 5.80^{a}
SD	81.93 ± 1.81^{bc}	7.55 ± 1.10^{b}	28.00 ± 5.55^{c}	7.59 ± 2.42^{bc}
SHD	82.61 ± 1.84^{b}	7.50 ± 1.49^{b}	31.59 ± 3.18^{b}	6.45 ± 2.76^{c}
HAD40	79.36 ± 4.86^{bc}	8.31 ± 1.57^{ab}	32.63 ± 2.27^{b}	8.75 ± 2.80^{bc}
HAD60	78.46 ± 5.09^{c}	8.71 ± 1.70^{ab}	36.10 ± 0.87^{a}	10.50 ± 2.33^{ab}

Note: L* indicates brightness (higher = brighter). a* represents the red–green axis: positive = red, negative = green; larger absolute value = more vivid. b* represents the yellow–blue axis: positive = yellow, negative = blue; larger absolute value = more vivid. ΔE is a comprehensive index calculated from L, a, and b*; a larger ΔE indicates a more obvious color difference. Numbers are shown as mean ± standard deviation. Different superscript letters within the same column indicate significant differences ($p < 0.05$) as determined by one-way ANOVA combined with Tukey's HSD post hoc test.

In terms of total color difference (ΔE) for fresh samples, the SHD-treated samples had the lowest ΔE values, indicating the least color change, while the FD-treated samples had the highest ΔE values. However, fresh slices are not the target product; therefore, a lower ΔE value does not necessarily indicate better quality. Instead, optimal color quality is determined based on visual consistency with the description in the pharmacopoeia. The second part of the Chinese Pharmacopoeia in 2025 records that the skin color of *Astragalus membranaceus* slices is light brownish-yellow or light brown, and the texture of the cut surface resembles "golden cups and silver plates" or "chrysanthemum hearts" [5]. Based on testing, the quality of the slices obtained using these three drying methods was relatively outstanding: HAD60 (rich deep yellow, L: 78.46 ± 5.09, a: 8.71 ± 1.70, b: 36.10 ± 0.87), SHD (bright golden yellow, L: 82.61 ± 1.84, a: 7.50 ± 1.49, b: 31.59 ± 3.18), and HAD40 (bright deep yellow, L: 79.36 ± 4.86, a: 8.31 ± 1.57, b*: 32.63 ± 2.27).

3.2. Effect of Different Drying Methods on the Microstructure of Astragalus membranaceus var. mongholicus Slices

3.2.1. FE-SEM Analysis

With the loss of water and heat migration during the drying process, the organization of the material will be affected by different degrees of changes in the microstructure. The microstructure of *Astragalus membranaceus* var. *mongholicus* slices under different drying conditions is shown in Figure 1 (magnification 100×). The results clearly indicate the presence of numerous vessels in the slices. However, no significant damage to the vascular structure was observed under any drying conditions. Minor variations in vessel diameter are not considered to be caused by the treatment methods, as these variations may stem from issues related to the sectioning plane or image resolution. A comparison of the number of blood vessels per unit area revealed that the vascular density resulting from the SD, SHD, and FD treatments was higher than that resulting from the hot air drying treatment. This result indicates that hot air drying causes greater damage to the vascular structure. Similarly, Lewicki et al. observed significant rupture and folding in the cell walls of apples dried by hot air [23]. For *Astragalus membranaceus* var. *mongholicus* slices, the disrupted cellular structure facilitates the dissolution of bioactive components.

At higher magnifications (500×, Figure S2), a large number of starch granules can be observed near the conduits. The number of visible intact starch granules varies depending on the drying method: compared to samples treated with SHD and FD, fewer starch granules were observed in samples treated with SD (see Figure S2A) and in samples treated with hot air drying (see Figure S2D,E). Recent investigations into the gelatinization behavior of legume starches have demonstrated that, within the temperature range of 50–60 °C, the process is primarily characterized by water absorption and granule expansion [24]. Therefore, the reduced visibility of starch in sun-dried and hot-air-dried samples is likely attributable to gelatinization, which alters granule morphology and makes them less discernible under SEM.

3.2.2. 3D Optical Profile Analysis

The morphological changes of fresh and differently dried *Astragalus membranaceus* var. *mongholicus* slices were further observed using a 3D optical profiler, and the results are shown in Figure 1. In 3D contour images, the red and blue areas represent extremely high surface protrusions and deep surface cavities, respectively. It can be seen that the SHD (Figure 1H) and HAD40/60 (Figure 1J,K) samples showed significant unevenness. The Ra parameter generally reflects the roughness of the sliced surface. As shown in Figure 1F, there were significant differences in Ra parameters for different drying methods ($p < 0.05$). The HAD40 treatment had the highest Ra value (50.73 μm) compared to the other treatments. In contrast, the slices treated with HAD60 exhibited a relatively smoother

surface due to starch gelatinization caused by the higher temperature, which filled their surface voids [19]. Compared to other treatments, SD surfaces exhibit the smoothest and most even texture without distinct peak–valley structures (Figure 1F,G). This is because the SD drying process involves gradual natural dehydration, which may promote uniform cell shrinkage and minimize localized collapse or wrinkling [25].

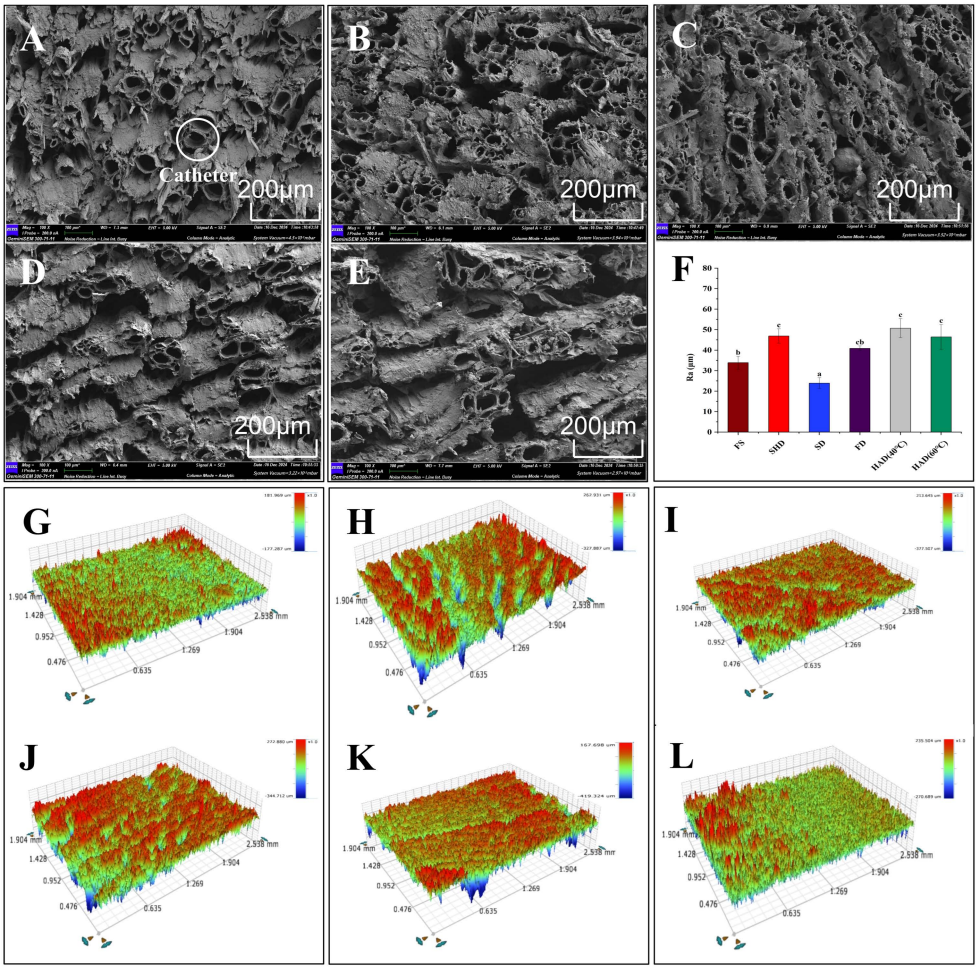

Figure 1. FE-SEM micrographs (100×, **A**–**E**), surface roughness (**F**), and 3D optical profiles (**G**–**L**) of *Astragalus membranaceus* var. *mongholicus* slices under different drying methods: (**A**,**G**) sun drying (SD); (**B**,**H**) shade drying (SHD); (**C**,**I**) freeze drying (FD); (**D**,**J**) hot air drying at 40 °C (HAD40); (**E**,**K**) hot air drying at 60 °C (HAD60); (**L**) fresh sample (FS). Different lowercase letters in (**F**) indicate significant differences ($p < 0.05$, one-way ANOVA with Tukey's HSD).

3.3. Effect of Different Drying Methods on the Relative Signal Intensity of Volatile Components in Astragalus membranaceus var. mongholicus Slices

3.3.1. GC-IMS Mapping Analysis of Volatile Components of *Astragalus membranaceus* var. *mongholicus* Slices from Different Drying Methods

In recent years, gas chromatography–ion mobility spectrometry (GC-IMS) has been widely applied in distinguishing the effects of different drying methods on traditional Chinese medicine [26]. In this study, GC-IMS technology was employed to analyze *Astragalus membranaceus* var. *mongholicus* slices subjected to different drying methods to investigate the effect of drying methods on volatile substances in the slices. As a purely observational description, Figure S3A shows the two-dimensional GC-IMS spectrum of volatile components. The color represents the peak intensity of the substances, ranging from blue to red, with darker colors indicating higher peak intensities. To further visually compare the differences in volatile components in *Astragalus membranaceus* var. *mongholicus* slices

under different drying methods, FS was selected as the reference, and the spectra of other samples were subtracted from the reference to obtain the differential comparison diagram, as shown in Figure 2B. Moreover, the three-dimensional chromatograms obtained by gas chromatography–ion mobility spectrometry for *Astragalus membranaceus* var. *mongholicus* slices processed by different drying methods are shown in Figure S3B. Based on visual inspection of Figures 2B and S3A,B, it is observed that the volatile organic compounds present in the slices processed using different drying methods exhibit apparent differences in peak intensity and profile.

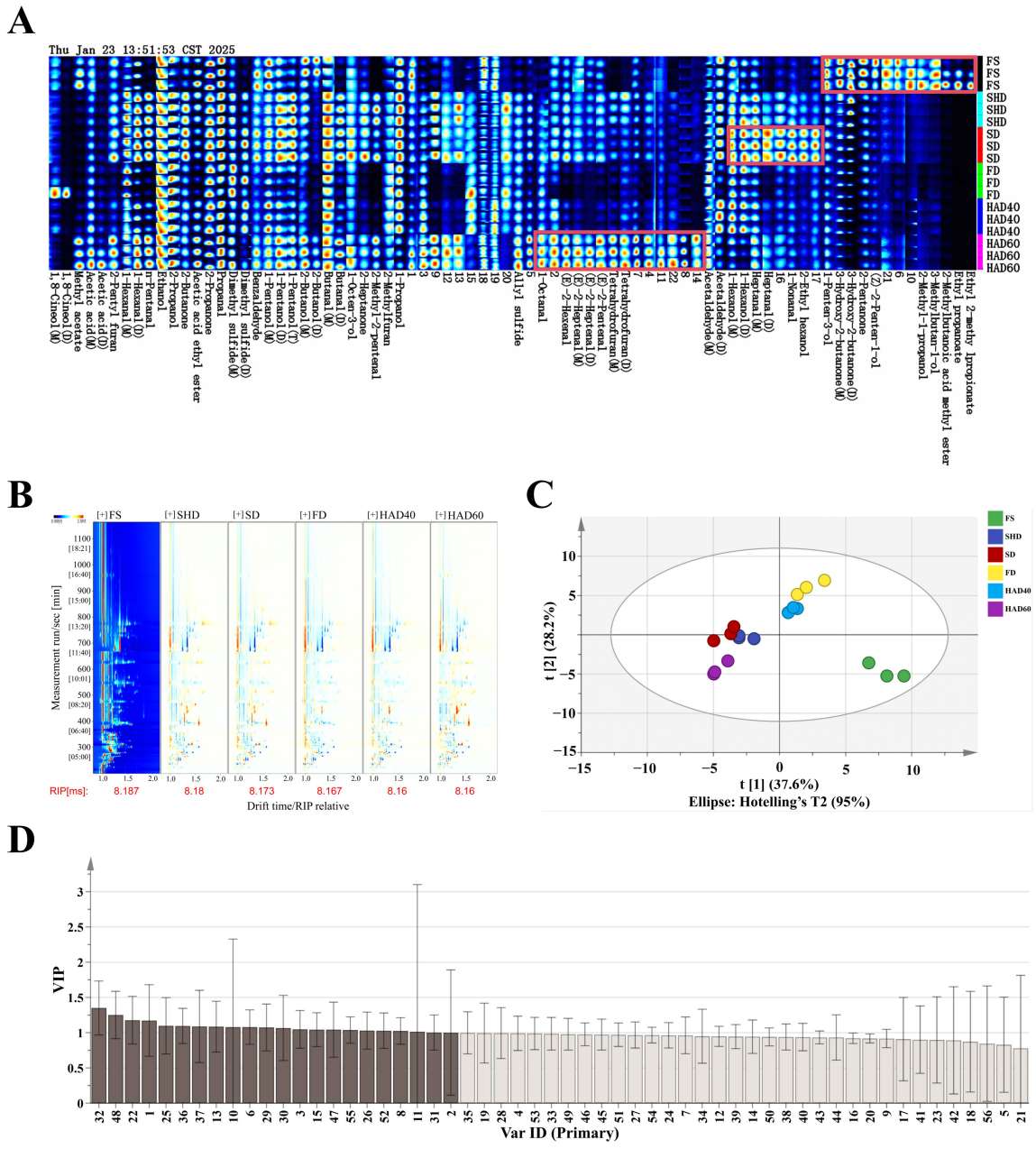

Figure 2. Three-dimensional GC-IMS spectral visualization and OPLS-DA analysis of volatile organic compounds under different drying treatments in *Astragalus membranaceus* var. *mongholicus* slices. (**A**) Heatmap of volatile compounds (columns) across drying methods (rows). Red = high intensity, blue = low. (**B**) Differential fingerprint against fresh sample (FS reference). (**C**) Plot of OPLS-DA scores. (**D**) Plot of VIP values. Lava-colored sections represent key difference compounds with VIP > 1. Note: The results of the one-way analysis of variance (ANOVA) and Tukey's HSD post hoc test indicate that only the relative signal intensities of chromatographic peaks 10, 11, and 21 did not differ significantly ($p < 0.05$).

Figure 2A shows the fingerprint of volatiles of *Astragalus membranaceus* var. *mongholicus* slices under different drying methods. From this observational fingerprint, the figure clearly displays the complete volatile organic compound information for each sample type, as well as the differences in volatile organic compounds between the samples. It is worth noting that visual inspection revealed that the relative signal intensities of C5–C9 aldehydes in the SD and HAD60 groups were significantly higher than those in the other treatment groups. A tentative interpretation, requiring further validation, is that their enrichment may suggest that the SD and HAD60 processes could have led to increased lipid oxidation in *Astragalus membranaceus* var. *mongholicus* slices due to excessive temperature or light exposure [27,28]. However, this mechanistic hypothesis should be distinguished from the direct observational data, as the current results do not prove causation.

3.3.2. GC-IMS Combined with OPLS-DA to Analyze the Volatile Fingerprints and Markers of *Astragalus membranaceus* var. *mongholicus* Slices Driven by Different Drying Methods

The volatile compounds and their relative signal intensities of six types of *Astragalus membranaceus* var. *mongholicus* slices were analyzed by the GC-IMS technique in this study. As shown in Table 2, a total of 56 chromatographic peaks were detected, corresponding to 42 unique volatile compounds (monomers, dimers, and trimers of the same compound are counted as one chemical substance). The between-group differences were further parsed by the OPLS-DA model, and the results are shown in Figure 2C. The slices from different drying methods showed significant grouping characteristics. The close clustering of FD and HAD40 samples and the near overlap of samples within the HAD40 group suggests that the compound composition is highly homogeneous under this method's conditions. SHD, SD and HAD60 samples were clustered in the same region, where SHD and SD were spatially located in high proximity to each other, reflecting the high similarity of their volatile components. The model parameters show excellent performance ($R^2X = 0.916$, $R^2Y = 0.939$, $Q^2 = 0.885$), all of which are above the discriminant model validity threshold (>0.5), and Hotelling's T2 analysis verifies that all samples are within the 95% confidence intervals, which suggests that the model has strong explanatory power and predictive ability. To verify the reliability of the model, the risk of overfitting was assessed by a 200-permutation test (Figure S4). The results show that all R^2 and Q^2 are below the value of replacement retention equal to 1.0 and the intercept of the Q^2 regression line is negative (−0.8), which meets the discriminant criterion of no overfitting (intercept < 0), confirming the robustness of the models [29].

Screening for key differential compounds (threshold VIP > 1) based on variable importance projection (VIP), 22 markers were identified (Figure 2D), covering alcohols (six types), aldehydes (six types), ketones (two types), esters (one type), carboxylic acids (two types), sulfides (two types) and ethers (three types). Specifically: acetic acid (M/D), 1-hexanol (M), 1-nonanal, 3-hydroxy-2-butanone (D), 1,8-cineol (M/D), heptanal (D), 1-hexanal (M), ethanol, acetic acid ethyl ester, 2-propanone, dimethyl sulfide, and 1-propanone, hexanal (M), ethanol, acetic acid ethyl ester, 2-propanone, dimethyl sulfide (M/D), acetaldehyde (M/D), 2-ethyl hexanol, 1-pentanol (M), tetrahydrofuran (D), 1-octen-3-ol, 2-methyl-2-pentenal and 1-propanol. The aforementioned volatile compounds (with the exception of 1,8-cineole ((M/D), $p > 0.05$) can serve as characteristic markers for distinguishing between different drying methods and will be used in subsequent multidimensional analysis and comprehensive evaluation. It is important to note that, while these markers are statistically discriminative, their biological or chemical interpretation requires additional experimental validation to establish mechanistic links.

Table 2. Detailed List of Volatile Components in *Astragalus membranaceus* var. *mongholicus* slices.

Number	Compound	CASNo.	Formula	MW	RI	Rt (s)	Dt (RIPrel.)	Flavor Description
1	Acetic acid (M)	C64197	$C_2H_4O_2$	60.1	1455.0	957.577	1.05086	spicy
2	Acetic acid (D)	C64197	$C_2H_4O_2$	60.1	1455.6	959.091	1.15098	spicy
3	1-Hexanol (M)	C111273	$C_6H_{14}O$	102.2	1362.7	772.804	1.32755	fresh, fruity, wine, sweet, green
4	1-Hexanol (D)	C111273	$C_6H_{14}O$	102.2	1365.1	776.397	1.64466	fresh, fruity, wine, sweet, green
5	(Z)-2-Penten-1-ol	C1576950	$C_5H_{10}O$	86.1	1332.4	728.663	0.95523	green, plastic, rubber
6	1-Nonanal	C124196	$C_9H_{18}O$	142.2	1396.4	826.739	1.48089	rose, citrus, strong oily
7	3-Hydroxy-2-butanone (M)	C513860	$C_4H_8O_2$	88.1	1297.9	681.4	1.05659	butter, cream
8	3-Hydroxy-2-butanone (D)	C513860	$C_4H_8O_2$	88.1	1294.8	677.329	1.35003	butter, cream
9	2-Pentyl furan	C3777693	$C_9H_{14}O$	138.2	1239.5	587.985	1.26417	bean, fruity, earthy, green, vegetable
10	1,8-Cineol (M)	C470826	$C_{10}H_{18}O$	154.3	1204.1	536.864	1.2958	camphor, refreshing herbal
11	1,8-Cineol (D)	C470826	$C_{10}H_{18}O$	154.3	1204.2	536.948	1.73939	camphor, refreshing herbal
12	Heptanal (M)	C111717	$C_7H_{14}O$	114.2	1187.7	514.677	1.35639	fresh, aldehyde, fatty, green herbs, wine, fruity
13	Heptanal (D)	C111717	$C_7H_{14}O$	114.2	1188.0	515.074	1.71221	fresh, aldehyde, fatty, green herbs, wine, fruity
14	1-Penten-3-ol	C616251	$C_5H_{10}O$	86.1	1160.0	475.205	0.95008	ethereal, green, tropical fruity
15	1-Hexanal (M)	C66251	$C_6H_{12}O$	100.2	1090.7	386.62	1.2874	fresh, green, fat, fruity
16	1-Hexanal (D)	C66251	$C_6H_{12}O$	100.2	1090.7	386.62	1.57524	fresh, green, fat, fruity
17	2-Methyl-1-propanol	C78831	$C_4H_{10}O$	74.1	1097.4	394.386	1.36997	fresh, alcoholic, leather
18	2-Methylbutanoic acid methyl ester	C868575	$C_6H_{12}O_2$	116.2	1014.1	326.685	1.547	apple
19	2-Pentanone	C107879	$C_5H_{10}O$	86.1	991.0	310.728	1.37157	acetone, fresh, sweet fruity, wine
20	n-Pentanal	C110623	$C_5H_{10}O$	86.1	992.0	311.384	1.43937	green grassy, faint banana, pungent
21	Ethyl 2-methylpropionate	C97621	$C_6H_{12}O_2$	116.2	976.4	301.984	1.57496	sweet, fruity, alcoholic, rummy
22	Ethanol	C64175	C_2H_6O	46.1	947.4	285.974	1.13124	aromaticity
23	2-Propanol	C67630	C_3H_8O	60.1	937.1	280.514	1.22363	alcohol, spicy
24	2-Butanone	C78933	C_4H_8O	72.1	926.2	274.86	1.25836	fruity, camphor
25	Acetic acid ethyl ester	C141786	$C_4H_8O_2$	88.1	904.3	266.454	1.34866	fresh, fruity, sweet, grassy
26	2-Propanone	C67641	C_3H_6O	58.1	833.7	247.053	1.12217	fresh, apple, pear
27	Methyl acetate	C79209	$C_3H_6O_2$	74.1	853.2	252.266	1.20287	ester, green
28	Propanal	C123386	C_3H_6O	58.1	816.0	242.419	1.15072	pungent, green grassy
29	Dimethyl sulfide (M)	C75183	C_2H_6S	62.1	792.6	236.404	0.95732	cabbage, sulfur, gasoline
30	Dimethyl sulfide (D)	C75183	C_2H_6S	62.1	789.8	235.704	1.13137	cabbage, sulfur, gasoline
31	Acetaldehyde (M)	C75070	C_2H_4O	44.1	756.0	227.315	0.96638	green, slight fruity
32	Acetaldehyde (D)	C75070	C_2H_4O	44.1	758.1	227.839	1.14367	green, slight fruity
33	(E)-2-Heptenal (M)	C18829555	$C_7H_{12}O$	112.2	1328.7	723.49	1.26167	spicy, green vegetables, fresh, fatty
34	(E)-2-Heptenal (D)	C18829555	$C_7H_{12}O$	112.2	1328.6	723.224	1.68304	spicy, green vegetables, fresh, fatty
35	Benzaldehyde	C100527	C_7H_6O	106.1	1493.1	1053.552	1.15911	bitter almond, cherry, nutty
36	2-Ethyl hexanol	C104767	$C_8H_{18}O$	130.2	1483.0	1027.13	1.41281	citrus, fresh floral, greasy
37	1-Pentanol (M)	C71410	$C_5H_{12}O$	88.1	1265.5	628.628	1.25983	balsamic
38	1-Pentanol (D)	C71410	$C_5H_{12}O$	88.1	1265.2	628.198	1.51603	balsamic
39	1-Pentanol (T)	C71410	$C_5H_{12}O$	88.1	1265.0	627.767	1.63297	balsamic
40	2-Butanol (M)	C78922	$C_4H_{10}O$	74.1	1032.6	340.022	1.14889	fruity
41	2-Butanol (D)	C78922	$C_4H_{10}O$	74.1	1030.7	338.615	1.3221	fruity
42	Butanal (M)	C123728	C_4H_8O	72.1	900.8	265.457	1.10738	pungent, fruity, green leaf
43	Butanal (D)	C123728	C_4H_8O	72.1	900.8	265.457	1.28858	pungent, fruity, green leaf
44	3-Methylbutan-1-ol	C123513	$C_5H_{12}O$	88.1	1213.3	549.636	1.49427	whiskey, banana, fruity
45	2-Methylfuran	C534225	C_5H_6O	82.1	872.5	257.53	0.98517	chocolate, ether like odor

Table 2. *Cont.*

Number	Compound	CASNo.	Formula	MW	RI	Rt (s)	Dt (RIPrel.)	Flavor Description
46	Tetrahydrofuran (M)	C109999	C_4H_8O	72.1	868.9	256.536	1.0671	ether
47	Tetrahydrofuran (D)	C109999	C_4H_8O	72.1	868.9	256.536	1.22725	ether
48	1-Octen-3-ol	C3391864	$C_8H_{16}O$	128.2	1451.1	948.181	1.16959	mushroom, lavender, rose, hay
49	1-Octanal	C124130	$C_8H_{16}O$	128.2	1290.5	670.442	1.40127	aldehyde, waxy, citrus, orange, fruity, fatty
50	(E)-2-Hexenal	C6728263	$C_6H_{10}O$	98.1	1227.5	570.148	1.52939	green, banana, fat
51	2-Heptanone	C110430	$C_7H_{14}O$	114.2	1183.1	508.69	1.64531	pear, banana, fruity, slight medicinal fragrance
52	2-Methyl-2-pentenal	C623369	$C_6H_{10}O$	98.1	1151.9	463.853	1.49966	aldehydes, soil, garlic, ripe cherries, fruity
53	Allyl sulfide	C592881	$C_6H_{10}S$	114.2	1144.8	454.219	1.32867	garlic
54	(E)-2-Pentenal	C1576870	C_5H_8O	84.1	1136.6	443.176	1.37307	potato, peas
55	1-Propanol	C71238	C_3H_8O	60.1	1041.8	346.85	1.2601	alcohol, pungent
56	Ethyl propanoate	C105373	$C_5H_{10}O_2$	102.1	938.0	280.997	1.45069	grape, pineapple, fruity, rum

Note: In the name of this compound, M, D, and T represent monomers, dimers, and trimers, respectively. Due to concentration effects in the IMS ion source, these substances with different structures actually all originate from the same chemical compound. Therefore, these 56 chromatographic peaks actually correspond to 42 different volatile compounds. All compounds are putative identifications at MSI Level 2 and have not been confirmed using chemical standards.

3.4. The Effect of Different Drying Methods on the Antioxidant Capacity of Astragalus membranaceus var. mongholicus Slices

Given that a single antioxidant assay cannot systematically assess the antioxidant capacity of plants, this study employed three different methods (ABTS, FRAP, and DPPH) to evaluate the antioxidant activity of dried *Astragalus membranaceus* var. *mongholicus* slices. However, it is important to note that these three assays are based on distinct reaction mechanisms (e.g., DPPH and ABTS methods measure radical scavenging capacity, while the FRAP method measures reducing power) and therefore should not be interpreted as interchangeable indicators of overall antioxidant capacity without further discussion. In addition, studies have shown that total phenols, total sugars, and total flavonoids in plants are associated with antioxidant capacity [18,30]. Accordingly, this study measured the changes in these components. Figure 3A–F shows the effect of different drying methods on the antioxidant capacity of *Astragalus membranaceus* var. *mongholicus* slices. The results showed that SHD had good DPPH radical scavenging activity with a scavenging rate of 64.89%, while HAD60 showed the lowest scavenging rate of 17.22%. A possible explanation for this observation is that moderate heating may improve the clearance rate, but excessively high temperatures could cause the decomposition of antioxidants, thereby reducing free radical scavenging capacity [31]. HAD40 treatment showed a relatively high ABTS radical scavenging capacity (46.05%), comparable to HAD60 (44.11%) and SHD (42.92%) with no statistically significant differences among the top three (Figure 3B). The effectiveness of all treatments is as follows in descending order: HAD40 (46.05%) > HAD60 (44.11%) > SHD (42.92%) > SD (41.59%) > FD (36.09%). Similarly, the SHD treatment yielded the highest FRAP content, reaching 1.47 μmol/mL, followed by other treatments in descending order: SHD (1.47 μmol/mL) > HAD60 (1.40 μmol/mL) > FD (1.35 μmol/mL) > HAD40 (1.29 μmol/mL) > SD (1.21 μmol/mL). Consistent with the findings of Xue et al., different drying conditions led to variations in DPPH and ABTS values [31]. In summary, all three antioxidant capacities of *Astragalus membranaceus* var. *mongholicus* slices are significantly altered by the drying method, and the mechanisms underlying each assay appear to be sensitive to the specific drying conditions applied.

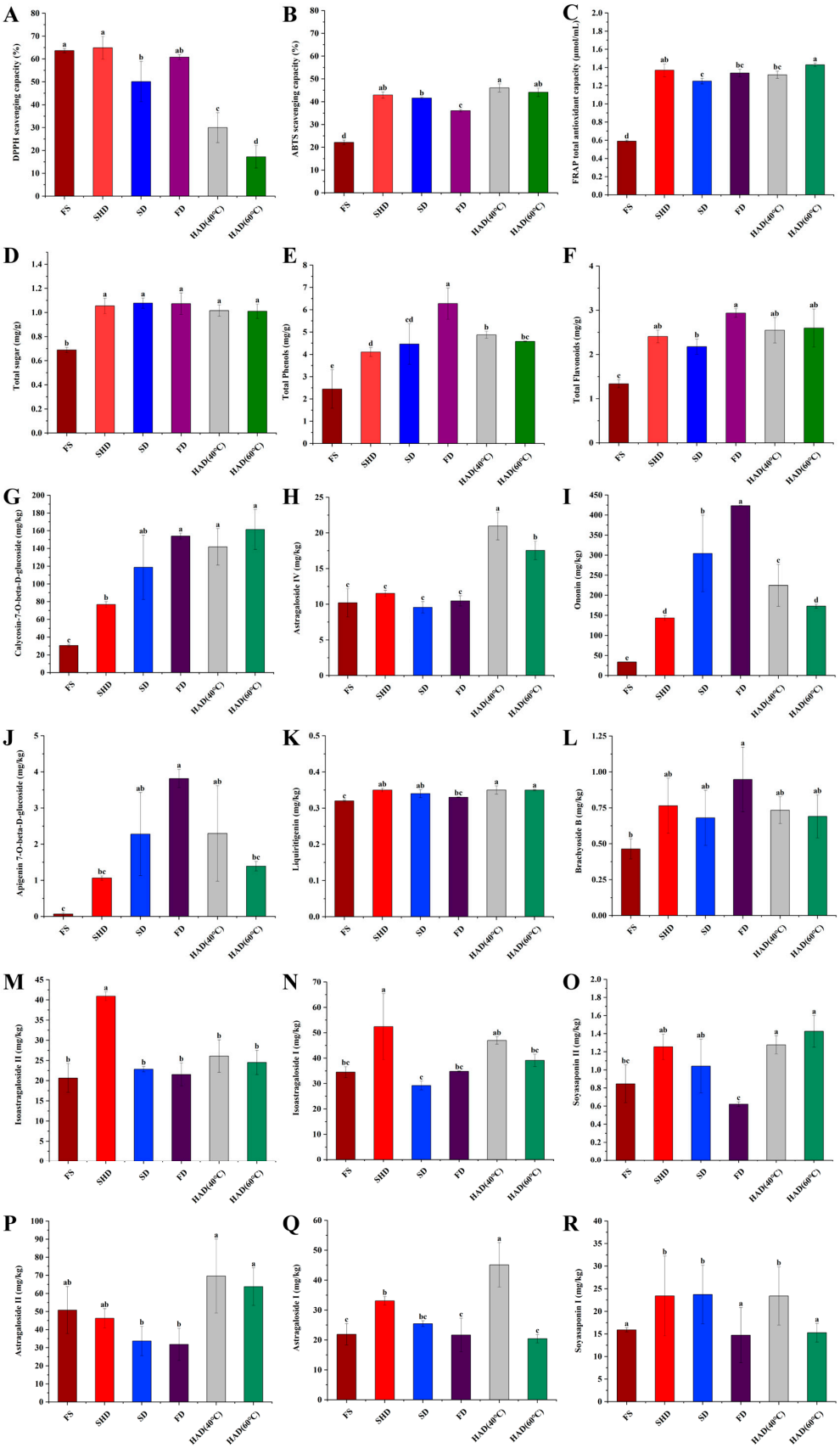

Figure 3. Effects of different drying methods on antioxidant capacity and active constituent contents in *Astragalus membranaceus* var. *mongholicus* slices. (**A**–**C**) Antioxidant assays: (**A**) DPPH, (**B**) ABTS, (**C**) FRAP. (**D**–**F**) Total contents: (**D**) sugars, (**E**) phenols, (**F**) flavonoids. (**G**–**R**) Individual active constituents (structures and identification in Supplementary Materials). Different lowercase letters indicate significant differences ($p < 0.05$, one-way ANOVA with Tukey's HSD).

As shown in Figure 3D–F, no significant differences were observed in total sugar content among the different drying methods, as the levels were similar across all groups. The study by Yang et al. indicated that water loss in plants leads to a gradual increase in the concentration of soluble sugars within cellular tissues [32]. Sugar metabolism during all drying methods may be dominated by water loss and thus no significant differences can be observed. The FD sample had the highest total phenolic content (6.27 mg/g, $p < 0.05$). The total phenolic contents of the other four treatment methods were, in descending order: HAD40 (4.87 mg/g) > HAD60 (4.58 mg/g) > SD (4.46 mg/g) > SHD (4.10 mg/g). The total flavonoid content was highest in both the FD and HAD40 samples (2.94 mg/g, $p < 0.05$). The total flavonoid contents of the other three treatment methods were, in descending order: HAD60 (2.55 mg/g) > SHD (2.34 mg/g) > SD (1.95 mg/g). Xing et al. similarly found that FD samples had the highest total phenolic content, followed slightly by oven drying, in their study of perilla leaves [33]. We present these measurements as observational data. While the trends in total phenols, flavonoids, and sugars co-vary with some antioxidant assays, we have not established causal relationships.

3.5. Effect of Different Drying Methods on the Content of Active Constituents of Astragalus membranaceus var. mongholicus Slices

The active constituents in traditional Chinese medicinal herbs are closely related to their therapeutic effects, and some of these active constituents are even used as quality markers (Q-markers) to evaluate the quality of Chinese medicinal herbs [17]. A total of 13 representative active constituents were detected in this study, and the UPLC-MS/MS ion flow chromatogram of these active constituent mixture controls is shown in Figure S5. The m/z values of the UPLC-MS/MS peaks for the active constituents are listed in Table S2. The results showed that, except for orientin (Figure S6), the other 12 active constituents showed significant differences between different drying methods (Figure 3G–R). Compared with FS, the content of astragaloside I, astragaloside II, soyasaponin I, and soyasaponin II in FD-treated *Astragalus membranaceus* var. *mongholicus* slices was reduced. In contrast, the content of these active components in slices treated with other drying methods was higher than that in the FS-treated group. Compared with other drying methods, FD resulted in relatively lower retention levels for certain saponins, although it exhibited advantages in preserving other components such as total phenolics. Kim et al. showed similar results in *ginseng* adventitious roots [34]. The contents of astragaloside IV and calycosin-7-O-β-D-glucoside in the hot-air-dried samples were significantly higher than those in the other samples (Figure 3G,H, $p < 0.05$). Notably, they are the only key active ingredients of *Astragalus membranaceus* to be detailed in the 2025 edition of the Chinese Pharmacopoeia [5]. This indicates that hot air drying has significant advantages in retaining the key active constituents of *Astragalus membranaceus* var. *mongholicus* slices.

3.6. Multivariate Analyses Revealing the Effect of Drying Method on Key Active Constituents and Antioxidant Activity in Astragalus membranaceus var. mongholicus Slices

3.6.1. Principal Component Analysis Reveals Differential Effects of Drying Methods on Saponin Retention and Antioxidant Capacity

Previous studies have shown that the antioxidant capacity of *Astragalus membranaceus* is significantly and positively correlated with the abundance and diversity of active constituents it contains [35]. This section systematically evaluates the effects of different drying methods on the retention rate of active constituents and antioxidant activity in *Astragalus membranaceus* var. *mongholicus* slices using principal component analysis (PCA). As shown in Figure 4A, the PCA results revealed that the cumulative contribution rate of the first two principal components reached 74.6%, sufficiently explaining the variation characteristics within the dataset. Specifically, Principal Component 1 (PC1, accounting for 46.7% of the

variance) exhibited significant positive correlations with antioxidant indices (FRAP, ABTS) and active constituents (total flavonoids, calycosin-7-O-β-D-glucoside) on its positive side ($PC1^+$) (Figure 4B). This indicates that $PC1^+$ comprehensively characterizes the antioxidant potential of the slices and the retention level of its glycoside components. Principal Component 2 (PC2, accounting for 27.9% of the variance) was strongly associated with saponin components (soyasaponin II, astragaloside II, isoastragaloside I, astragaloside IV) on its positive side ($PC2^+$). This indicates that $PC2^+$ reflects the stability of saponin constituents.

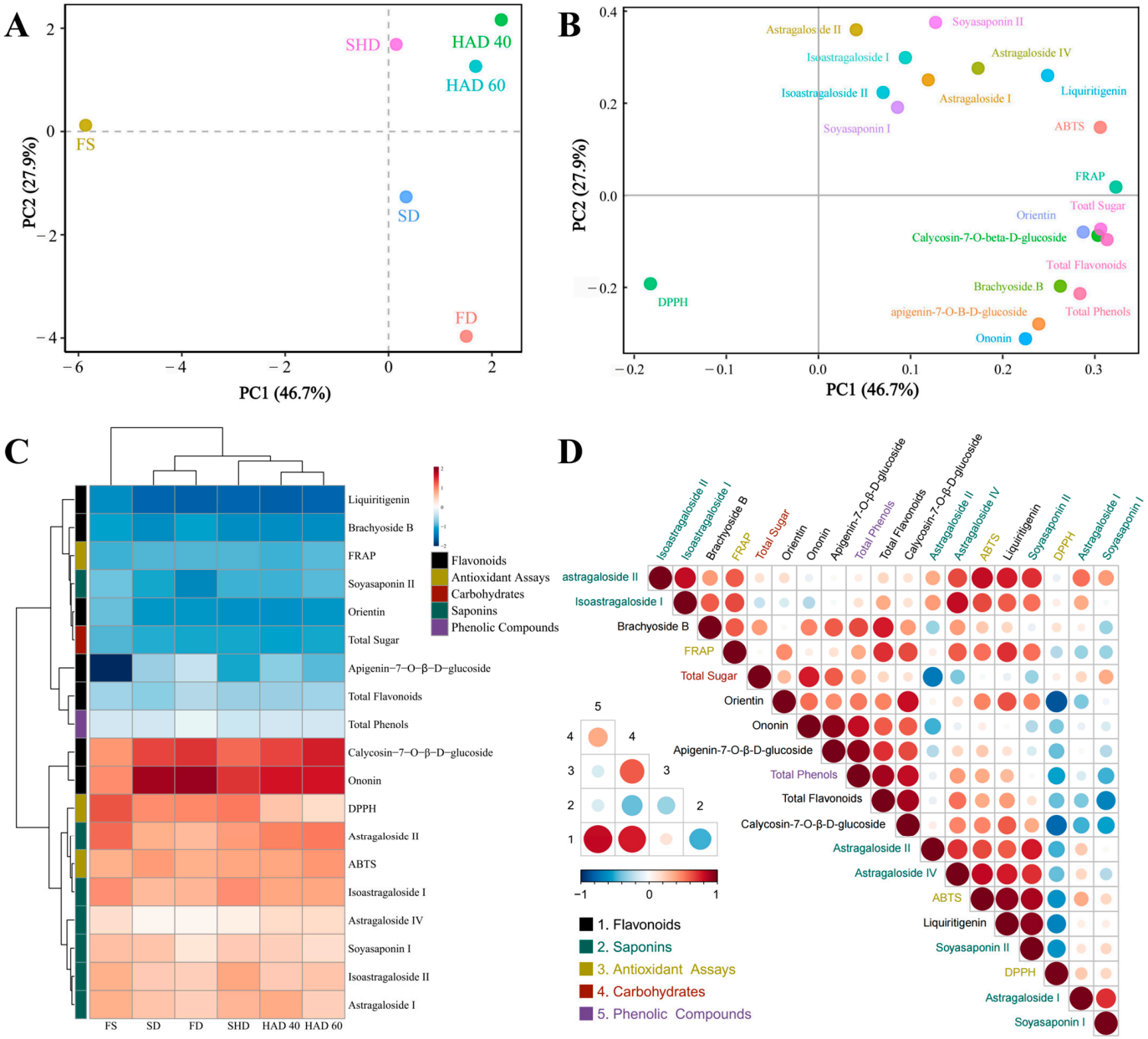

Figure 4. Multivariate analyses revealing the effect of drying method on bioactive components and antioxidant activity in *Astragalus membranaceus* var. *mongholicus* slices. (**A**) Principal component score plot. (**B**) Principal component loading plot. (**C**) Hierarchical clustering heatmap of active constituents and antioxidant activity, rows and columns were clustered based on correlation distance and average linkage. Red = high activity, blue = low. (**D**) Heatmap of correlation analysis between active constituents and antioxidant activity. Large heatmap: Pairwise correlation matrix between individual bioactive constituents and antioxidant activities across all samples. Small heatmap: Correlation matrix between grouped categories (Flavonoids, Saponins, Antioxidant assays, Carbohydrates, Phenolic compounds).

Further analysis revealed that SHD, HAD40, and HAD60 samples were all distributed within the $PC1^+/PC2^+$ quadrant, suggesting they simultaneously exhibit higher antioxidant activity and saponin retention. Among them, HAD40, HAD60, and SHD all fell within the $PC1^+/PC2^+$ quadrant, indicating generally higher antioxidant activity and saponin retention compared to SD and FD. However, no single method outperformed others across all metrics: SHD had the highest FRAP, FD had the highest total phenols, and HAD40 showed competitive ABTS and certain glycoside components. These findings are consistent with the conclusions of Salamatullah et al., indicating that hot air drying is relatively superior to other drying methods in preserving the antioxidant capacity of certain plants and minimizing the loss of specific bioactive compounds [36]. In summary, HAD40 is a balanced choice that provides competitive performance in ABTS and certain saponins and glycosides, but it is not superior across all dimensions.

3.6.2. Component-Specific Retention Patterns and Inter-Component Interactions in *Astragalus membranaceus* var. *mongholicus* Slices of Different Drying Methods Revealed by Clustering and Correlation Analysis

Cluster analysis of *Astragalus membranaceus* var. *mongholicus* slices subjected to different drying treatments (Figure 4C) revealed a distinct classification pattern, SD and FD clustered together, HAD40 and HAD60 formed another distinct group, while SHD and FS constituted independent clusters. This clustering outcome exhibited strong correspondence with the spatial distribution observed in Figure 4A, further corroborating the systematic impact of the drying methods on the chemical composition of the samples. Compared with the FS group, the dried treatment group exhibited a significant increase in flavonoid glycoside content, such as calycosin-7-O-β-D-glucoside, ononin, and apigenin-7-O-β-D-glucoside, while the content of liquiritigenin was markedly reduced. Existing studies have confirmed the significant pharmacological activities of these compounds. Calycosin-7-O-β-D-glucoside inhibits lipid accumulation in hepatocytes by activating the AMPK signaling pathway [37]; ononin demonstrated significant anti-cancer potential in in vitro models [38]; the inhibitory effect of apigenin-7-O-β-D-glucoside on lipopolysaccharide-induced inflammation has been verified through animal experiments [39]; and liquiritigenin may ameliorate renal inflammation by suppressing inflammasome activation [40]. These results collectively indicate that the drying method effectively preserves the pharmaceutically active constituents of *Astragalus membranaceus* var. *mongholicus* slices.

To elucidate the variation patterns of chemical components and antioxidant properties during the drying process, this study further employed Spearman correlation analysis. The results revealed positive correlations between total flavonoid content and FRAP ($r = 0.71$) and ABTS ($r = 0.37$). This finding aligns with the conclusions of Bozkuş et al., regarding the strong positive correlation between flavonoids and antioxidant activity in honey [41]. Notably, most saponin components (e.g., astragaloside I, isoastragaloside II) not only clustered together but also exhibited strong associations with antioxidant indices such as DPPH and ABTS in Figure 4C. Among these, the linkage between isoastragaloside I and ABTS was particularly pronounced. Similarly, Zhang et al. demonstrated that the scavenging efficiency of oat saponins against DPPH radicals, hydroxyl radicals (OH), and superoxide anions (O_2^-) exhibits a dose-dependent positive correlation with their concentration [42]. However, as shown in Figure 4D, partial saponin components (e.g., astragaloside I: $r = -0.31$, soyasaponin I: $r = -0.31$) exhibited negative correlations with FRAP. This indicates that the relationship between saponins and antioxidant capacity in the slices is complex and multidimensional. Furthermore, total sugar content exhibited a strong positive correlation with antioxidant indices ($r = 0.60$), suggesting that saccharides may enhance antioxidant capacity through synergistic effects with phenolics and flavonoids [43]. This implies that

total sugar could serve as an effective indicator for assessing the antioxidant potential of *Astragalus membranaceus* var. *mongholicus* slices.

3.7. Multidimension Analysis Revealing the Effect of Drying Method on Quality of Astragalus membranaceus var. mongholicus Slices

3.7.1. Network Analysis Suggests a Potential Cascading Regulatory Hypothesis for Quality Attributes Driven by HAD40 in *Astragalus membranaceus* var. *mongholicus* Slices

To comprehensively characterize the effects of different drying methods on *Astragalus membranaceus* var. *mongholicus* slices, this study constructed an interaction network ($p < 0.05$, $|r| > 0.75$) based on Spearman correlation analysis (Figure 5A, Table S3). This network encompassed four color characteristic indicators, three microstructure indicators, 13 active constituents, six antioxidant indicators, and the 56 chromatographic peaks (representing 42 volatile compounds) of the slices. The interaction network revealed high consistency among the microscopic morphology parameters of the slices: Ra with Rp (r = 0.94), Ra with Rq (r = 0.94), and Rp with Rq (r = 1). This indicates that these parameters can serve as reliable indicators for characterizing the physical properties of the slices. All microscopic morphology parameters showed significant positive correlations with isoastragaloside I and astragaloside IV ($p < 0.05$, $r > 0.75$), and it is speculated that an increase in the surface roughness of the slices may improve the content of these two compounds. The antioxidant activity of astragaloside IV has been widely demonstrated [44,45]. In this study, the content of astragaloside IV was directly and positively correlated with ABTS radical scavenging capacity (r = 0.83). The ABTS capacity was negatively correlated with 1,8-cineole (M) (r = −0.89) but positively correlated with allyl sulfide (r = 0.89) and liquiritigenin (r = 0.94). This suggests that volatile compounds like cineole may exert antagonistic effects on antioxidant activity, while sulfide and flavonoid compounds may synergistically enhance this activity [46,47]. Rodenak-Kladniew et al. further demonstrated that 1,8-cineole—the primary component isolated from eucalyptus essential oil—induces reactive oxygen species (ROS) generation, consistent with its potential antioxidant-antagonistic effects [48]. Interestingly, total flavonoid content showed a positive correlation with acetaldehyde (r = 0.94) but negative correlation with 1-penten-3-ol (r = −0.94). The accumulation of flavonoids concomitant with an increase in oxidation products (acetaldehyde) implies that they may function not only as antioxidants but also as responsive molecules to oxidative stress within the system. The color difference index ΔE exhibited exceptionally strong positive correlations with total flavonoids (r = 0.94), total phenolics (r = 0.94), and calycosin-7-O-β-D-glucoside (r = 0.94). Furthermore, ΔE increased synchronously with Maillard reaction markers, acetaldehyde (r = 0.89) and 2-methylfuran (r = 0.83), but showed negative correlations with 1-penten-3-ol (r = −0.89) and 3-hydroxy-2-butanone (r = −0.94). In summary, as a comprehensive color index, ΔE shows a strong correlation with both oxidation products (Maillard reaction) and antioxidants (flavonoids/phenolics) and may directly reflect the redox state of the system. Therefore, we speculate that ΔE can serve as an important indicator for assessing the redox state of the slices.

Based on the observed strong correlations (roughness vs. astragaloside IV: r = 0.94; astragaloside IV vs. ABTS: r = 0.83; ABTS vs. b*: r = 0.89), we hypothesize a potential cascading relationship: coarsening of microstructure → increased astragaloside IV content → enhanced antioxidant activity → changed color characteristics (e.g., b*). However, it should be emphasized that these correlations do not demonstrate causation, as all variables might be independently influenced by processing temperature and other drying conditions. Therefore, this proposed cascade should be regarded as a working hypothesis rather than a demonstrated mechanism. Further experimental validation (e.g., pathway inhibition or genetic manipulation) is required to establish causality.

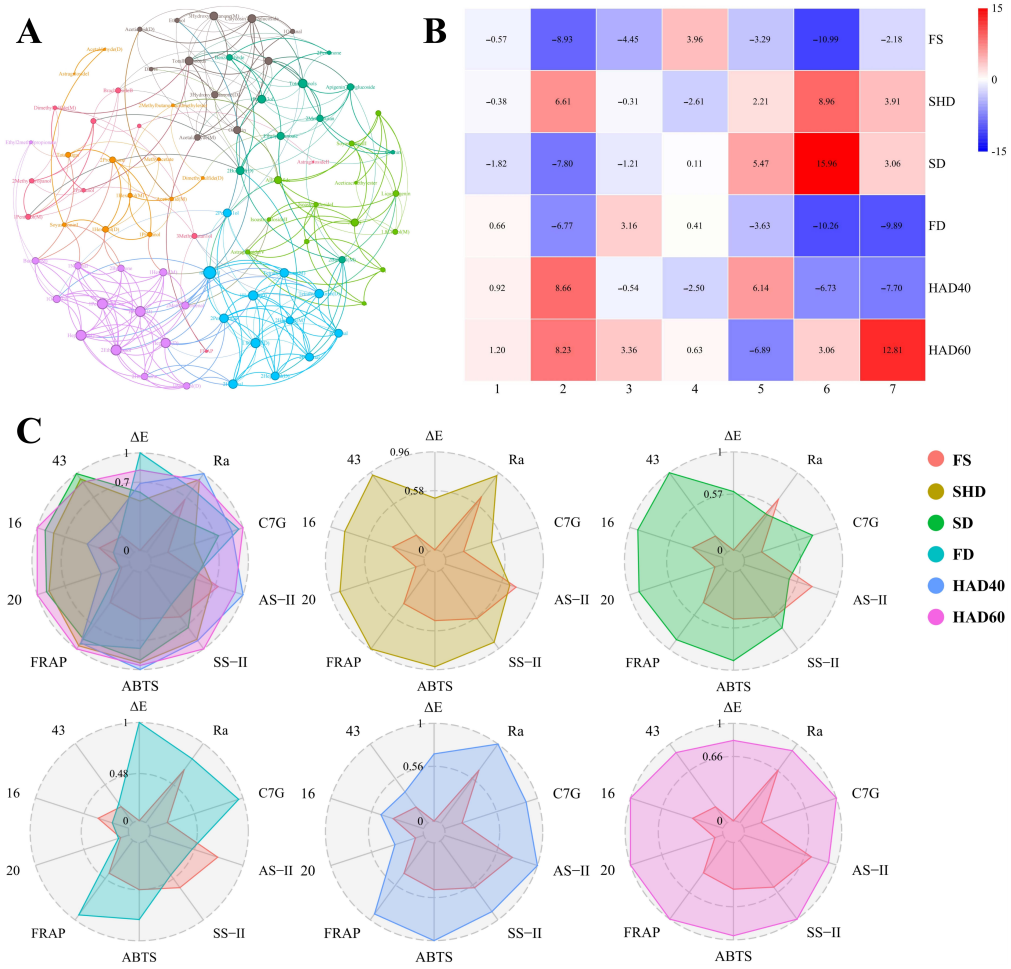

Figure 5. Network analysis and comprehensive evaluation of functional attributes and quality indicators in *Astragalus membranaceus* var. *mongholicus* slices subjected to different drying methods. (**A**) Interaction network of functional modules in *Astragalus membranaceus* var. *mongholicus* slices ($|r| > 0.75$, $p < 0.05$). Different colors represent different modules. Node size reflects connectivity. (**B**) Expression profiles of functional modules under different drying methods. (**C**) Radar chart for multiparametric comprehensive evaluation. C7G: calycosin-7-O-β-D-glucoside; AS-II: astragaloside II; SS-II: soyasaponin II; 20: n-pentanal; 16: 1-hexanal (D); 43: butanal (D).

3.7.2. The Functional Module Expression Spectrum Clearly Demonstrates the Excellent Characteristics of HAD40 Samples

Based on the interactive network, seven functional modules were identified by the Leiden algorithm according to the functional characteristics of each indicator. The network exhibited significant modularity, with a modularity value greater than 0.3 (Q = 0.597). The specific composition of each module is detailed in Tables S4 and S5. To elucidate the response characteristics of different functional modules to drying methods, module expression profiles were further plotted, providing a visual representation of the overall expression patterns of each module under different drying methods (Figure 5B). As shown in Table S5, Functional Module 1 integrates color parameters (L*, a*), saponin active constituents (astragaloside II, brachyoside B), antioxidant capacity (FRAP), and C3-C5 alcohol volatiles. This module reveals an association between color changes, saponin transformation, and the generation of small-molecule alcohol volatiles. Functional Module 2 aggregates microstructure parameters (Ra, Rp, Rq), multiple saponins (five types), and a strong antioxidant indicator (ABTS) and is associated with sulfur-containing volatiles (allyl sulfide). This suggests that alterations in microstructure may influence saponin release and antioxidant activity, while sulfides could be key carriers of characteristic flavor compounds formed during

drying. This module reflects the association between microstructural changes, saponin release, and antioxidant activity. In Functional Module 3, the color difference indicator (ΔE) showed coordinated associations with flavonoid glycosides (calycosin-7-O-β-D-glucoside, luteolin-7-O-glucoside) and antioxidant indicators (total flavonoids, DPPH) and drove the variations of volatiles such as acetaldehyde and ethanol. This module suggests that changes in color difference are significantly associated with the transformation of flavonoid glycosides and that acetaldehyde-type compounds may originate from the oxidative degradation of flavonoids. This module points to an integrated process involving antioxidant activity, flavonoid glycoside transformation, and acetaldehyde metabolism. Functional Module 4 aggregated flavonoid glycosides (ononin, apigetrin), total phenolics, benzaldehyde, and furan-type volatiles (e.g., 2-methylfuran). This indicates that phenolic acids and flavonoid glycosides may synergistically contribute to antioxidant activity, while furan compounds may reflect pyrolytic products of glycosides. This module represents flavonoids, phenolic acids, and their associated furan derivatives. Functional Module 5 demonstrated strong associations among saponins (astragaloside I, soyasaponin I), total sugars, pyruvate-related metabolites, and acetic acid volatiles. This module suggests that saponins and sugars may share biosynthetic pathways, while pyruvate-derived metabolites indicate glycolytic activity. This module primarily links saponins, sugar moieties, and products related to pyruvate metabolism. Functional Module 6 was significantly enriched with C6-C10 aldehydes and ketones. These long-chain carbonyl compounds are characteristic products of lipid oxidation, reflecting the extent of lipid degradation during drying. Functional Module 7 primarily comprised oxidative end products of polyunsaturated fatty acids (PUFAs), whose variations directly correlate with thermal stress during drying.

As shown in Figure 5B, *Astragalus membranaceus* var. *mongholicus* slices samples subjected to different drying methods exhibited significant differences in expression levels across the functional modules. SHD samples showed high expression in Modules 2, 6, and 7. This indicates that the process is significantly correlated with increased microstructural roughness of the slices (Module 2), enhanced lipid degradation (Module 6), and the oxidation of polyunsaturated fatty acids (PUFAs) (Module 7). SD samples exhibited significantly elevated expression levels in Module 6, which may indicate that the process is significantly associated with the promotion of lipid degradation. FD samples demonstrated very low expression levels in Modules 2, 6, and 7. This indicates that the process is strongly correlated with the inhibition of lipid degradation (Module 6), the oxidation of polyunsaturated fatty acids (PUFAs) (Module 7), and the reduction of microsurface roughness and saponin release on the slices (Module 2). HAD40 samples exhibited strong expression in Modules 2 and 5. This indicates that the process is strongly associated with increasing the microscopic roughness of the slice surface, promoting the release of saponins, enhancing antioxidant activity (Module 2), and boosting activities related to saponins, glycosylated groups, and pyruvate metabolism (Module 5). Notably, HAD40 showed expression patterns consistent with a positive role in the proposed cascading network. HAD40 samples exhibited high expression in Modules 2 and 5, which include microstructure parameters, astragaloside IV, and antioxidant indicators, supporting the hypothesis that HAD40 may enhance these linked attributes. However, this interpretation remains correlative. Furthermore, HAD40 samples showed low expression levels in Modules 6 and 7. This suggests that it may effectively inhibit lipid degradation (Module 6) and PUFA oxidation (Module 7). Compared with the HAD40 samples, the HAD60 samples showed a significantly weaker correlation with antioxidant activity (associated with Modules 2 and 5) but a significantly stronger correlation with lipid degradation (Module 6) and polyunsaturated fatty acid (PUFA) oxidation (Module 7). This indicates that excessively high drying temperatures may have compromised the overall quality of the slices. In conclusion, within the framework of our

multidimensional evaluation, the HAD40-treated *Astragalus membranaceus* var. *mongholicus* slices demonstrated the most balanced overall quality profile.

3.7.3. Multiparametric Evaluation Validates HAD40 as the Optimal Drying Method for Astragalus membranaceus var. mongholicus Slices

To enable an objective comparison of various drying methods, we first defined "overall quality" for *Astragalus membranaceus* var. *mongholicus* slices as a balanced profile that prioritizes: (1) retention of pharmacopoeial bioactive components (astragaloside IV and calycosin-7-O-β-D-glucoside); (2) antioxidant capacity; (3) minimal lipid oxidation; (4) appropriate physical microstructure (related to extractability); and (5) color consistency with pharmacopoeial description. Within this definition, pharmacopoeial markers and antioxidant activity were given primary importance because they directly relate to efficacy, while color and physical microstructure were secondary but still considered. No explicit weighting was applied beyond equal contribution of each selected indicator in the scoring formula. The rationale for selecting each specific indicator is as follows: the ΔE value is the indicator that best reflects quality in color analysis. Additionally, network analysis results show a strong correlation between ΔE and total flavonoids, total phenolic compounds, and calycosin-7-O-β-D-glucoside (all with an r value of 0.94). Furthermore, the ΔE value also reflects the progression of the Maillard reaction. Therefore, the ΔE value is the indicator that best reflects the overall redox state of the sample. The Ra value reflects physical roughness, which directly affects the elution of active compounds; moreover, it exhibits a significant positive correlation with astragaloside IV and isoastragaloside I (r values greater than 0.75). This association suggests that surface roughness may be related to the extractability or retention of key saponins, although further experimental validation is required. Regarding antioxidant capacity, we simultaneously employed the ABTS method (for detecting free radical scavenging capacity) and the FRAP method (for detecting reducing capacity), as these two methods can measure different antioxidant mechanisms, respectively. Combining these two detection methods yields more accurate and comprehensive evaluation results than relying on a single indicator alone. Among them, the three active components had the highest PCA loadings (see Section 3.6.1), and these components are precisely the saponins and flavonoids with the most significant pharmacological effects. Additionally, these three aldehydes were the compounds with the highest loadings in the OPLS-DA analysis; as indicators of lipid oxidation, they reflect the extent of thermal oxidation of lipids during the drying process.

During data normalization, each parameter is converted into a percentage value relative to the best-performing sample. For indicators where "higher values are better" (Ra, the three active ingredients, ABTS, FRAP), the formula for calculating the standardized value (%) is: (X/Xmax) × 100%. For indicators where "lower values are better" (ΔE, the three aldehydes), the formula for calculating the standardized value (%) is: (X/Xmax) × 100%. The composite score for each drying method is calculated using the following formula: Σ(standardized values of "higher-is-better" indicators) − Σ(standardized values of "lower-is-better" indicators). Here, Ra, the three active ingredients, ABTS, and FRAP are all "higher-is-better" indicators, while ΔE and the three aldehydes are "lower-is-better" indicators.

The radar chart (Figure 5C) provides a visual overview of the numerical values for each metric. No single method outperforms the others across all metrics: for example, FD has the lowest ΔE value, indicating the strongest color retention; while HAD60 has the highest FRAP value. However, HAD40 demonstrated the most balanced performance across all metrics: it ranked among the top in Ra value, active ingredient content, and antioxidant capacity, while also maintaining low ΔE values and relative signal intensity of aldehydes. The scores for each metric are as follows: HAD40 scored 3.85 points, FD scored

2.84 points, HAD60 scored 2.07 points, SHD scored 1.71 points, SD scored 0.79 points, and FS scored 2.45 points (for reference only).

HAD40 achieved the highest composite score (3.85), primarily because it simultaneously ranked among the top two in all three "higher-is-better" categories (Ra, active components, antioxidant capacity) while also scoring well in the "lower-is-better" categories (low ΔE and low aldehydes). In contrast, FD had excellent ΔE and total phenolics but scored lower on saponins and ABTS; SHD had high FRAP but higher aldehydes (lipid oxidation); HAD60 had high FRAP but higher ΔE and aldehydes. Thus, HAD40's advantage lies in its balanced performance without major weaknesses. However, this conclusion is contingent on our definition of overall quality. If a different application prioritizes total phenolics over saponins, FD may be preferable; if maximum reducing power is the sole goal, HAD60 could be chosen. The scoring system and data are provided transparently to allow alternative interpretations. This conclusion is consistent with the analysis results regarding functional module expression in Section 3.7.2: HAD40 activates the 2nd and 5th beneficial functional modules while simultaneously inhibiting the 6th and 7th functional modules associated with lipid oxidation.

3.8. Scope of the Current Study and Considerations for Future Work on Multiscale Imaging

This study establishes a multidimensional evaluation framework for comparing drying methods. Several aspects deserve further investigation. First, continuous monitoring of drying kinetics in future studies would enable correlation between dehydration rates and retention of bioactive components. Second, controlled environment studies would help deconvolute the individual effects of temperature, light, and airflow—particularly for natural drying methods. Third, full analytical validation (e.g., intra-day/inter-day precision for UPLC-MS/MS, authentic standards for GC-IMS markers, multiscale imaging at different magnifications) would strengthen future method robustness. Fourth, the correlative cascade hypothesis (roughness → astragaloside IV → antioxidant activity) requires direct experimental testing, such as surface modification or controlled extraction studies. Fifth, additional quality attributes—energy consumption, rehydration capacity, microbial stability, and sensory properties—could be integrated into future comprehensive assessments. Finally, multibatch and multiorigin validations are needed to confirm the general applicability of the observed drying method ranking.

4. Conclusions

This study systematically evaluated five drying methods for *Astragalus membranaceus* var. *mongholicus* slices using a multidimensional model (color, microstructure, volatiles, bioactive components, antioxidant activity). The main findings are: (1) drying methods differ significantly. No single method outperformed others across all indicators. Freeze drying preserved total phenolics best, while shade drying showed higher DPPH and FRAP values. (2) Hot air drying at 40 °C (HAD40) offers balanced performance. Under our predefined quality framework (prioritizing pharmacopoeial markers, antioxidant capacity, low lipid oxidation, microstructure and color), HAD40 achieved the highest composite score. It was associated with increased surface roughness, higher astragaloside IV and calycosin-7-O-β-D-glucoside levels, enhanced ABTS activity, and lower lipid-oxidation-related aldehydes. However, this ranking depends on the specific evaluation criteria. (3) Strong correlations were observed (roughness vs. astragaloside IV: r = 0.94; astragaloside IV vs. ABTS: r = 0.83). Based on this, we propose a testable hypothesis: HAD40 may improve saponin extractability/retention through surface roughening, thereby contributing to antioxidant activity. Direct experimental validation is needed.

Supplementary Materials: The following supporting information can be downloaded at: https://www.mdpi.com/article/10.3390/separations13050146/s1, Figure S1: The appearance of *Astragalus membranaceus* var. *mongholicus* slices under different drying treatments.; Figure S2: Microstructure of *Astragalus membranaceus* var. *mongholicus* slices under different drying conditions (Magnification 500×); Figure S3: Three-dimensional GC-IMS spectral visualization. (A) GC-IMS topographic map. (B) Three-dimensional spectra of different treatment drying methods; Figure S4: Plot of cross-validation of 200-substitution test; Figure S5: UPLC-MS/MS ion chromatogram of 13 active substance mixed control solutions in positive mode; Figure S6: The orientin content of different dried samples; Table S1: Calibration parameters, regression equations, and sensitivity for 13 active constituents by UPLC-MS/MS; Table S2: Mass spectral information and retention times for 13 *Astragalus membranaceus* var. *mongholicus* active substances; Table S3: Component composition of the 7 functional modules; Table S4: Structural composition of the 7 functional modules; Table S5: Component composition of the 7 functional modules.

Author Contributions: F.L.: Writing—original draft, Writing—review and editing, Visualization. J.W.: Experimental operation, Data curation, Writing—original draft, Writing—review and editing. L.H.: Experimental operation, Data curation, Writing—original draft. M.L.: Methodology, Experimental operation, Software, Funding acquisition, Writing—review and editing. Y.S.: Investigation, Visualization. Y.W.: Investigation, Visualization. J.C.: Resources, Methodology, Writing—review and editing. X.D.: Supervision, Writing—review and editing. B.M.: Investigation, Software, Writing—review and editing. Q.L.: Investigation, Software, Writing—review and editing. Z.K.: Resources, Supervision, Project administration, Funding acquisition, Writing—original draft, Writing—review and editing. All authors have read and agreed to the published version of the manuscript.

Funding: This study was supported by the Key Research and Development Program of Ningxia (2026FRF05002), the Ministry of Finance and Ministry of Agriculture and Rural Affairs: National Modern Agricultural Industry Technology System (CARS-21), the Major Science and Technology Project in Yunnan Province (202402AE090011), the first batch of "2 + 5" key talent plan in Xinjiang Uygur Autonomous Region.

Data Availability Statement: The original contributions presented in this study are included in the article/Supplementary Materials. Further inquiries can be directed to the corresponding authors.

Conflicts of Interest: The authors declare no conflict of interest.

References

1. Durazzo, A.; Nazhand, A.; Lucarini, M.; Silva, A.M.; Souto, S.B.; Guerra, F.; Severino, P.; Zaccardelli, M.; Souto, E.B.; Santini, A. *Astragalus* (*Astragalus membranaceus* Bunge): Botanical, geographical, and historical aspects to pharmaceutical components and beneficial role. *Rend. Lincei. Sci. Fis. Nat.* **2021**, *32*, 625–642. [CrossRef]
2. Chen, Z.J.; Liu, L.J.; Gao, C.F.; Chen, W.J.; Vong, C.T.; Yao, P.F.; Yang, Y.H.; Li, X.Z.; Tang, X.D.; Wang, S.P.; et al. Astragali radix (Huangqi): A promising edible immunomodulatory herbal medicine. *J. Ethnopharmacol.* **2020**, *258*, 112895. [CrossRef]
3. Riaz, A.; Rasul, A.; Hussain, G.; Zahoor, M.K.; Jabeen, F.; Subhani, Z.; Younis, T.; Ali, M.; Sarfraz, I.; Selamoglu, Z. Astragalin: A bioactive phytochemical with potential therapeutic activities. *Adv. Pharmacol. Sci.* **2018**, *2018*, 9794625. [CrossRef]
4. Dong, M.Y.; Li, J.J.; Yang, D.L.; Li, M.F.; Wei, J.H. Biosynthesis and pharmacological activities of flavonoids, triterpene saponins and polysaccharides derived from *Astragalus membranaceus*. *Molecules* **2023**, *28*, 5018. [CrossRef]
5. Chinese Pharmacopoeia Commission. *Chinese Pharmacopeia 2025*; China Medical Science Press: Beijing, China, 2025.
6. Hu, L.Z.; Li, M.M.; Sun, Y.W.; Zhao, H.R.; Chen, J.Y.; Dai, X.F.; Kong, Z.Q. Pesticide and mycotoxin residues in *Astragalus*: Transfer patterns, processing factors and risk assessment during *Astragalus* processing. *Food Chem.* **2025**, *81*, 144167. [CrossRef]
7. Zhu, L.Y.; Gong, H.; Gan, X.N.; Bu, Y.X.; Liu, Y.P.; Zhang, T.T.; Chen, J.; Xu, Y.B.; Shi, S.S.; Li, T.Z.; et al. Processing-structure-activity relationships of polysaccharides in chinese materia medica: A comprehensive review. *Carbohydr. Polym.* **2025**, *358*, 123503. [CrossRef] [PubMed]
8. Li, X.; Wang, Y.; Ma, X.; Li, M.; Kong, D.; Phavady, P.; Wang, Q.; Abdelkader, T.K. Chinese medicinal materials' drying technologies advancements—Principles, energy performance, and influence on the bioactive components. *Dry. Technol.* **2024**, *12*, 1815–1845. [CrossRef]
9. Lu, M.K.; Chang, C.C.; Chao, C.H.; Hsu, Y.C. Structural changes, and anti-inflammatory, anti-cancer potential of polysaccharides from multiple processing of *Rehmannia glutinosa*. *Int. J. Biol. Macromol.* **2022**, *206*, 621–632. [CrossRef] [PubMed]

10. Lu, J.D.; Wang, Z.; Qin, L.H.; Shen, J.Y.; He, Z.; Shao, Q.S.; Lin, D. Drying methods affect bioactive compound contents and antioxidant capacity of *Bletilla striata* (Thunb.) Reichb.f. flower. *Ind. Crops Prod.* **2021**, *164*, 113388. [CrossRef]
11. Park, J.; Park, D.; Lee, W. Quality change of sliced *ginseng* depending on different drying methods. *Food Sci. Preserv.* **2017**, *24*, 361–366.
12. Jana, S.N.; Datta, A.S.; Santra, K.; Rahman, S.M.; Rashid, M.H.A. An overview of the importance of quality evaluation and validation of medicinal plants. *Int. J. Green. Pharm.* **2026**, *19*, 193–203.
13. Chen, Q.P.; Xie, Q.; Li, W.Y.; Wang, C.H. Research progress and prospect on quality grade standards of Chinese medicinal materials and TCM decoction pieces. *Shanghai J. Tradit. Chin. Med.* **2022**, *57*, 87–95.
14. Li, Y.Q.; He, X.H.; Wu, G.S.; Man, J.H.; Zhang, X.C.; Wang, Z.X. Effect of drying method on the major active components, in vitro antioxidant activity, α-glucosidase inhibitory activity, volatile components, and metabolites of *Panax notoginseng* leaves. *Food Sci.* **2023**, *44*, 98–113.
15. Sun, Y.; Lin, L.; Zhang, P. Color development kinetics of Maillard reactions. *Ind. Eng. Chem. Res.* **2021**, *9*, 3495–3501. [CrossRef]
16. Karunasena, H.C.P.; Hesami, P.; Senadeera, W.; Gu, Y.T.; Brown, R.J.; Oloyede, A. Scanning electron microscopic study of microstructure of gala apples during hot air drying. *Dry. Technol.* **2014**, *4*, 455–468. [CrossRef]
17. Kang, T.G.; Dou, D.Q.; Xu, L. Establishment of a quality marker (Q-marker) system for Chinese herbal medicines using burdock as an example. *Phytomedicine* **2019**, *54*, 339–346. [CrossRef]
18. Akther, S.; Jothi, J.S.; Badsha, M.R.; Rahman, M.M.; Das, G.B.; Alim, M.A. Drying methods effect on bioactive compounds, phenolic profile, and antioxidant capacity of mango powder. *J. King Saud. Univ. Sci.* **2023**, *35*, 102370. [CrossRef]
19. Wu, Z.; Gao, R.P.; Li, H.; Liao, X.; Tang, X.; Wang, X.G.; Su, Z.M. How steaming and drying processes affect the active compounds and antioxidant types of *Gastrodia elata* Bl. *f. glauca S. chow*. *Food Res. Int.* **2022**, *157*, 111277. [CrossRef]
20. Sumner, L.W.; Amberg, A.; Barrett, D.; Beale, M.H.; Beger, R.; Daykin, C.A.; Fan, T.W.M.; Fiehn, O.; Goodacre, R.; Griffin, J.L.; et al. Proposed minimum reporting standards for chemical analysis. *Metabolomics* **2007**, *3*, 211–221. [CrossRef] [PubMed]
21. Al-Abbasy, O.Y.; Younus, S.A.; Rashan, A.I.; Ahmad, O.A.S. Maillard reaction: Formation, advantage, disadvantage and control. A review. *Food Sci. Appl. Biotechnol.* **2024**, *7*, 145–161. [CrossRef]
22. Shengbu, M.; Ai, L.; Shi, Q.; Lai, X.R. Research progress of maillard reaction and its application in processing of traditional Chinese medicine. *Nat. Prod. Commun.* **2024**, *19*, 1934578X241290620. [CrossRef]
23. Lewicki, P.P.; Pawlak, G. Effect of drying on microstructure of plant tissue. *Dry. Technol.* **2003**, *4*, 657–683. [CrossRef]
24. Zhang, X.; Zhu, C.; Geng, D.; Cheng, Y.; Tang, N. Characterization of dynamic of the structural changes of legume starches during gelatinization. *Int. J. Biol. Macromol.* **2025**, *296*, 139673. [CrossRef]
25. Mayor, L.; Sereno, A.M. Modelling shrinkage during convective drying of food materials: A review. *J. Food Eng.* **2004**, *61*, 373–386. [CrossRef]
26. Gao, L.; Yang, R.W.; Li, L.Q.; Han, B.; Kai, G.Y. Application of gas chromatography-ion mobility spectrometry in traditional Chinese medicines: A review. *J. Appl. Res. Med. Aromat. Plants* **2025**, *46*, 100632. [CrossRef]
27. Reza, F. Critical kinetic parameters and rate constants representing lipid peroxidation as affected by temperature. *Food Chem.* **2021**, *340*, 128137. [CrossRef]
28. Qiu, D.; Duan, R.; Wang, Y.Q.; He, Y.F.; Li, C.; Shen, X.R.; Li, Y.C. Effects of different drying temperatures on the profile and sources of flavor in semi-dried golden pompano (*Trachinotus ovatus*). *Food Chem.* **2023**, *401*, 134112. [CrossRef]
29. Qian, S.Z.; Jiang, Y.M.; Yan, Q.L.; Wu, D.H.; Zhang, W.X.; Chung, J.P. Visualization OPLS class models of GC-MS-based metabolomics data for identifying agarwood essential oil extracted by hydro-distillation. *Sci. Rep.* **2025**, *15*, 5421. [CrossRef]
30. Augustin, S.; Ian, T.J.; Mike, S. Polyphenols: Antioxidants and beyond. *Am. J. Clin. Nutr.* **2005**, *81*, 2155–2175. [CrossRef] [PubMed]
31. Xue, T.T.; Ruan, K.H.; Xu, H.B.; Liu, H.B.; Tang, Z.S.; Yang, Y.G.; Duan, J.A.; Sun, X.X.; Wang, M.; Song, Z.X. Effect of different drying methods on the drying characteristics, chemical properties and antioxidant capacity of *Ziziphus jujuba* var. Spinosa fruit. *LWT-Food Sci. Technol.* **2024**, *196*, 115873. [CrossRef]
32. Yang, F.F.; Wang, Q.J.; Liu, W.Y.; Xiao, H.W.; Hu, J.Q.; Duan, X.J.; Sun, X.Y.; Liu, C.J.; Wang, H.O. Changes and correlation analysis of volatile flavor compounds, amino acids, and soluble sugars in durian during different drying processes. *Food Chem. X* **2024**, *21*, 101238. [CrossRef] [PubMed]
33. Xing, Y.; Lei, H.J.; Wang, J.; Wang, Y.T.; Wang, J.H.; Xu, H.D. Effects of different drying methods on the total phenolic, rosmarinic acid and essential oil of purple perilla leaves. *J. Essent. Oil-Bear. Plants* **2017**, *20*, 1594–1606. [CrossRef]
34. Kim, S.J.; Murthy, H.N.; Hahn, E.J.; Lee, H.L.; Paek, K.Y. Effect of processing methods on the concentrations of bioactive components of ginseng (*Panax ginseng* C.A. Meyer) adventitious roots. *LWT-Food Sci. Technol.* **2008**, *6*, 959–964. [CrossRef]
35. Yao, J.; Peng, T.; Shao, C.; Liu, Y.; Lin, H.; Liu, Y. The antioxidant action of Astragali radix: Its active components and molecular basis. *Molecules* **2024**, *29*, 1691. [CrossRef]
36. Salamatullah, A.M.; Ahmed, M.A.; Hayat, K.; Husain, F.M.; Arzoo, S.; Alzahrani, A.; Alotaibi, A.; Alyahya, H.K.; Ahmad, S.R. Different drying techniques effect on the bioactive properties of rose petals. *J. King Saud. Univ. Sci.* **2024**, *36*, 103025. [CrossRef]

37. Xu, W.; Zhou, F.; Zhu, Q.; Bai, M.; Luo, T.; Zhou, L.; Deng, R. Calycosin-7-O-β-D-glucoside attenuates palmitate-induced lipid accumulation in hepatocytes through AMPK activation. *Eur. J. Pharmacol.* **2022**, *925*, 174988. [CrossRef]
38. Sharma, U.; Sharma, B.; Mishra, A.; Sahu, A.; Mathkor, D.M.; Haque, S.; Raina, D.; Ramniwas, S.; Gupta, M.; Tuli, H.S. Ononin: A comprehensive review of anticancer potential of natural isoflavone glycoside. *J. Biochem. Mol. Toxicol.* **2024**, *38*, e23735. [CrossRef]
39. Hu, W.; Wang, X.; Wu, L.; Shen, T.; Ji, L.; Zhao, X.; Si, C.L.; Jiang, Y.; Wang, G. Apigenin-7-O-β-D-glucuronide inhibits LPS-induced inflammation through the inactivation of AP-1 and MAPK signaling pathways in RAW 264.7 macrophages and protects mice against endotoxin shock. *Food Funct.* **2016**, *7*, 1002–1013. [CrossRef]
40. Hongyan, L.; Suling, W.; Weina, Z.; Yajie, Z.; Jie, R. Antihyperuricemic effect of liquiritigenin in potassium oxonate-induced hyperuricemic rats. *Biomed. Pharmacother.* **2016**, *84*, 1930–1936. [CrossRef]
41. Bozkuş, T.N. Correlation of total polyphenol and flavonoid content with antioxidant activity of Caucasian bee honey. *Food Sci. Nutr.* **2025**, *13*, e4611. [CrossRef]
42. Zhang, L.; Li, J.; Huo, Y.; Yang, W.; Chen, J.; Gao, Z.; Yang, Z. Ultrasonic extraction and antioxidant evaluation of oat saponins. *Ultrason. Sonochem.* **2024**, *109*, 106989. [CrossRef]
43. Kopjar, M.; Lončarić, A.; Mikulinjak, M.; Šrajbek, Ž.; Šrajbek, M.; Pichler, A. Evaluation of antioxidant interactions of combined model systems of phenolics in the presence of sugars. *Nat. Prod. Commun.* **2016**, *11*, 1445–1448. [CrossRef] [PubMed]
44. Liang, Y.; Chen, B.; Liang, D.; Quan, X.; Gu, R.; Meng, Z.; Gan, H.; Wu, Z.; Sun, Y.; Liu, S.; et al. Pharmacological effects of Astragaloside IV: A review. *Molecules* **2023**, *28*, 6118. [CrossRef]
45. Liu, X.; Shang, S.; Chu, W.; Ma, L.; Jiang, C.; Ding, Y.; Wang, J.; Zhang, S.; Shao, B. Astragaloside IV ameliorates radiation-induced senescence via antioxidative mechanism. *J. Pharm. Pharmacol.* **2020**, *72*, 1110–1118. [CrossRef] [PubMed]
46. Smolyaninov, I.V.; Burmistrova, D.A.; Arsenyev, M.V.; Polovinkina, M.A.; Pomortseva, N.P.; Fukin, G.K.; Poddel'sky, A.I.; Berberova, N.T. Synthesis and antioxidant activity of new catechol thioethers with the methylene linker. *Molecules* **2022**, *10*, 3169. [CrossRef]
47. Matvieieva, N.; Drobot, K.; Duplij, V.; Ratushniak, Y.; Shakhovsky, A.; Kyrpa-Nesmiian, T.; Mickevičius, S.; Brindza, J. Flavonoid content and antioxidant activity of *Artemisia vulgaris* L. "hairy" roots. *Prep. Biochem. Biotechnol.* **2019**, *49*, 82–87. [CrossRef]
48. Rodenak-Kladniew, B.; Castro, A.; Stärkel, P.; Galle, M.; Crespo, R. 1,8-Cineole promotes G0/G1 cell cycle arrest and oxidative stress-induced senescence in HepG2 cells and sensitizes cells to anti-senescence drugs. *Life Sci.* **2020**, *243*, 117271. [CrossRef] [PubMed]